Imaging Drug Delivery to Skin with Stimulated Raman Scattering Microscopy

Brian G. Saar[1,†,‡], L. Rodrigo Contreras-Rojas[2,†], X. Sunney Xie[1,*], Richard H. Guy[2,*]

[1]Dept. of Chemistry and Chemical Biology, Harvard University, Cambridge, MA 02138, USA

[2]Dept. of Pharmacy & Pharmacology, University of Bath, Claverton Down, Bath, BA2 7AY, UK

[†]Equal contributors

[‡]Present address: MIT Lincoln Laboratory, 244 Wood Street, Lexington, MA 02420

[*]Address correspondence to these authors. E-mail: xie@chemistry.harvard.edu (X.S.X.); r.h.guy@bath.ac.uk (R.H.G.)

Abstract

Efficient drug delivery to the skin is essential for the treatment of major dermatologic diseases, such as eczema, psoriasis and acne. However, many compounds penetrate the skin barrier poorly and require optimized formulations to ensure their bioavailability. Here, stimulated Raman scattering (SRS) microscopy, a recently-developed, label-free chemical imaging tool, is used to acquire high resolution images of multiple chemical components of a topical formulation as it penetrates into mammalian skin. This technique uniquely provides label-free, non-destructive, three-dimensional images with high spatiotemporal resolution. It reveals novel features of (trans)dermal drug delivery in the tissue environment: different rates of drug penetration via hair follicles as compared to the intercellular pathway across the stratum corneum are directly observed, and the precipitation of drug crystals on the skin surface is visualized after the percutaneous penetration of the co-solvent excipient in the formulation. The high speed three-dimensional imaging capability of SRS thus reveals features that cannot be seen with other techniques, providing both kinetic information and mechanistic insight into the (trans)dermal drug delivery process.

Keywords

Skin; topical drug delivery; stimulated Raman scattering microscopy; skin penetration pathways; dermatopharmacokinetics.

TOC graphic

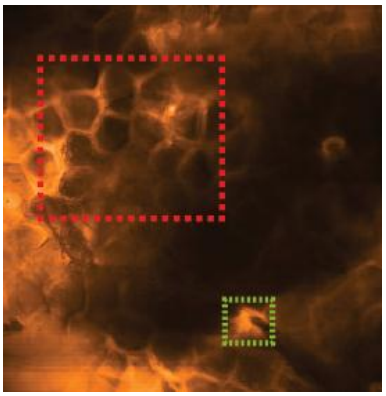

Abbreviations

AUC	area under the normalised SRS signal versus skin depth profile
CARS	coherent anti-Stokes Raman scattering
PG	propylene glycol
SC	stratum corneum
SRS	stimulated Raman scattering

Introduction

While the barrier properties of human skin are essential to life, the low permeability of this membrane to many compounds means that topical drug delivery to treat dermatological disease is very challenging[1]. To optimize the transport of skin-active compounds, analytical methods are required to determine the rate and extent of absorption into and through the barrier. At present, a widely-used approach involves adhesive tape-stripping[2], in which the outermost layer of skin (the stratum corneum (SC), which constitutes the principal barrier) is progressively removed and then analyzed chemically to produce the drug's concentration profile across the membrane. In contrast, an ideal technique would enable relevant measurements in mammalian skin and provide label-free, nondestructive analysis with high spatial and temporal resolution. Here, we demonstrate that stimulated Raman scattering (SRS) microscopy[3-7], a recently-developed imaging technique (**Figure 1**), is an ideal tool for this purpose, because it offers high sensitivity and high spatial resolution imaging of chemical distributions without the use of exogenous fluorescent labels.

Figure 1A shows the energy diagram of SRS. Two laser beams with frequencies ω_p (the pump beam) and ω_S (the Stokes beam) have a difference frequency ω_p-ω_S that matches an intrinsic molecular vibrational frequency in the sample at ω_{vib}. The SRS process transfers intensity from the pump beam to the Stokes beam and excites the vibrational resonance of the sample from the ground state (υ=0) to the first vibrational excited state (υ =1). **Figure 1B** then illustrates the principle of modulation transfer detection: Before the sample, the pump laser pulse train is unmodulated while the Stokes laser pulse train is modulated at a reference frequency of 10 MHz. After both beams interact with the sample, the Stokes beam is blocked by an optical filter and the pump beam is detected by a photodiode and lock-in amplifier. Because SRS only occurs when both beams are present, amplitude modulation of the Stokes beam is transferred to the pump beam (because SRS removes intensity from the pump beam) and can be sensitively detected.

In this work, two non-steroidal anti-inflammatory drugs, ibuprofen and ketoprofen, were evaluated following their topical application as solutions in propylene glycol (PG), a common co-solvent/excipient used in a wide variety of pharmaceutical, cosmetic and personal care formulations[1]. For SRS imaging, ketoprofen had a strong vibrational resonance from aromatic CH bond stretching at ~1599 cm^{-1}, while deuteration of PG and ibuprofen created unique vibrational resonances at approximately 2120 cm^{-1}. These Raman signals were easily distinguished (with minimal cross-talk given the ~5 cm^{-1} spectral resolution of the picosecond SRS imaging system used) from the strong spectral

fingerprint emanating from skin lipids, including those in the intercellular domains of the stratum corneum and those secreted by sebaceous glands (**Figure 1C**).

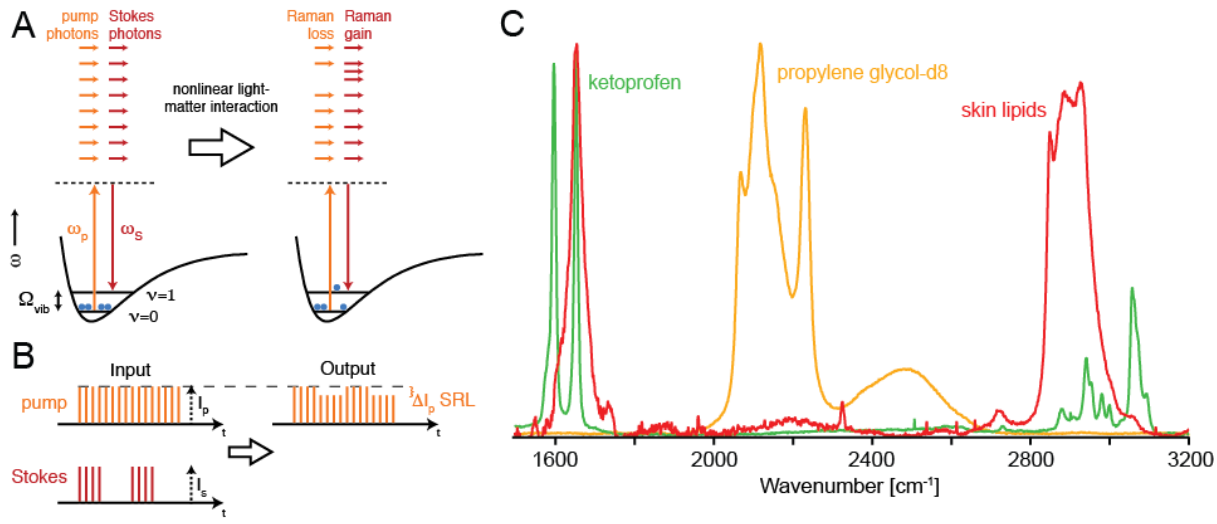

Figure 1: *Principle of SRS microscopy detection.* ***(A)*** *The energy diagram. During the SRS process, light is transferred from the pump beam to the Stokes beam, and the sample is vibrationally-excited.* ***(B)*** *Principle of modulation transfer detection.* ***(C)*** *Raman spectra used in this work. The contrast in SRS is based on the spontaneous Raman spectra, which are used to determine the optimal excitation wavelengths for SRS.*

Experimental Section

Solution Preparation. Ketoprofen (≥ 98% TLC), ibuprofen-d_3 (≥ 98% HPLC), propylene glycol (≥ 99.5% GC) and propylene glycol-d_8 (98 atom %D), were obtained from Sigma-Aldrich (Gillingham, Dorset, UK). For the experiments with ketoprofen, the drug was dissolved in propylene glycol-d_8 at a concentration of 180 mg ml^{-1}; i.e., at ~90% of its reported saturation solubility[8] of approximately 199 mg ml^{-1}. In the ibuprofen experiments, the deuterated drug was dissolved in ('normal', undeuterated) PG at a concentration of 380 mg ml^{-1}, which again represents about 90% of the published solubility (~430 mg ml^{-1})[9].

Raman Spectroscopy. Raman spectra (**Figure 1C**) of mouse skin and of the chemicals used in the study were acquired using a commercial Raman microspectrometer (LabRam HR, Horiba Jobin Yvon) with 633 nm excitation and detection via an open-electrode charge coupled device camera linked to a 750 mm focal length dispersive polychromator.

Sample Preparation. For imaging experiments, 7-9 week old BALB/c mice were purchased from a commercial supplier (Taconic) and housed in OAR-style facilities according to Harvard FAS IACUC Protocol #29-01. They were sacrificed using asphyxiation by CO_2 followed by cervical dislocation. All measurements reported here are performed *ex vivo*. The solutions were applied in a 25 µl aliquot to a small portion of an ear (~10 mm^2). The ear was sandwiched between a #1 coverslip and a microscope slide using double-sided adhesive (Grace Biolabs). The total ear thickness was less than 400 µm. The sample was placed on the stage of the SRS microscope and images were recorded as described below.

SRS Imaging. The SRS microscope was similar to one described previously,[4] and consisted of a picosecond-pulsed laser system pumping a modified laser scanning microscope optimized for SRS imaging. The laser system was based on a mode-locked Nd:YVO_4 laser (picoTrain, High Q Laser) that delivered 7 ps pulses at a repetition rate of 76 MHz with an average power of ~18W at 1064 nm. A portion of the fundamental output was used as the Stokes beam. The remainder of the output was frequency doubled and 6W of light at 532 nm was used to synchronously pump an optical parametric oscillator (OPO; Levante Emerald, APE GmbH). The OPO signal wave output was employed as the pump beam and was tunable from 680 nm to 1000 nm, allowing coverage of the vibrational spectrum from 600 cm^{-1} to >4000 cm^{-1} when combined with the 1064 nm Stokes beam. The spectral width in both beams was ~0.3 nm. The OPO was tuned using the integrated control electronics which allow the nonlinear crystal temperature, intra-cavity tuning element and cavity length to be adjusted with computer control.

The Stokes beam output passed through an electro-optic modulator based on a pair of rubidium titanyl phosphate crystals (Raicol Crystals, Ltd.), to which a high voltage sinusoidal drive waveform at 10 MHz was applied. The modulator, in combination with a polarization analyzer, provided amplitude modulation of the Stokes beam with ~100% modulation depth at the 10 MHz drive frequency. The Stokes beam and pump beam were combined on a dichroic mirror (DM; 1064dcrb, Chroma Technology) after the Stokes beam was delayed so that the two pulse trains temporally and spatially overlap after the DM. The combined beams were aligned into a modified upright laser scanning microscope (BX61WI/FV300, Olympus) with high near-infrared throughput. The two beams were focused into the sample (described above) using a water immersion objective lens (UPlanSApo 60X 1.2NA, Olympus) and scanned in two dimensions using a pair of galvanometer mirrors. The transmitted laser beams were collected using a high numerical aperture condenser (1.4NA, Nikon) and relayed using a pair of lenses onto a large-area photodiode (FDS1010, Thorlabs). An optical filter (CARS890/220, Chroma Technology) in front of the photodiode blocked the Stokes beam and transmitted the pump beam. The photodiode

was back-biased through a passive bandpass filter (BLP-1.9, Minicircuits) and the photocurrent was bandpass-filtered (BBP-10.7, Minicircuits) and fed in to a lock-in amplifier (SR844, Stanford Research Systems) for demodulation. The lock-in amplifier output, which was proportional to the SRS signal, was routed into the analog input of the microscope scan controller and displayed onscreen using the control PC and software (FV5, Olympus). Depth stacks were obtained by controlled movements of the objective lens using a stepper motor under control of the scan software.

Data Analysis. After data acquisition, three-dimensional images were analyzed using Igor Pro (Wavemetrics). The datasets were manually registered based on the appearance of the individual images and similar regions of interest were integrated to obtain the intensities as function of depth and location. For presentation of the image stacks, linear look-up tables were applied with different false color schemes to represent different Raman shifts.

Results & Discussion

First, a ketoprofen solution in deuterated PG was applied *ex vivo* to an excised piece of mouse ear, which was subsequently sealed between two coverslips and placed on the SRS microscope stage. Three-dimensional volumes of SRS data were then acquired over an area of approximately 250 x 250 μm^2 and to a depth of ~100 μm. The images obtained extended from within the drug-in-solvent layer above the skin down to the subcutaneous fat. The lipid architecture was first mapped from a series of images based on the CH_2 stretching absorbance at 2845 cm^{-1}. Attention was focused on the major barrier to skin penetration of chemicals, the SC (the outermost ~15 μm of the skin) which comprises tightly packed layers of terminally differentiated, keratin-filled corneocytes (roughly hexagonal in shape, ~20 μm across, yet only ~0.5 μm in thickness), the spaces between which are filled with a mixture of lipids organized into lamellar bilayers. SRS delineated individual cells clearly via the CH_2 signal emanating from the intercellular lipids (**Figure 2**) in the images recorded from different depths (Z), indicated down the left side of the figure, at the beginning (t = 11 minutes post-application of the ketoprofen in PG solution) and end (t = 158 minutes) of the penetration experiments. Registration of images to the same tissue region is possible, an attribute thereby permitting useful and novel mechanistic information to be deduced. An off-resonance image taken after the final CH_2-stretching dataset shows no signal, demonstrating the label-free contrast and chemical selectivity of SRS. When the pump laser is tuned off-resonance (i.e., away from the CH_2 stretching absorbance frequency), the signal level drops to the background which is

<1% of the peak CH_2 signal (and <5% of the peak signal from PG-d_8 discussed below), making the image effectively black and featureless. This outcome highlights a major advantage of SRS over the related coherent anti-Stokes Raman scattering (CARS) technique for which strong background signals from tissue complicate data analysis[4].

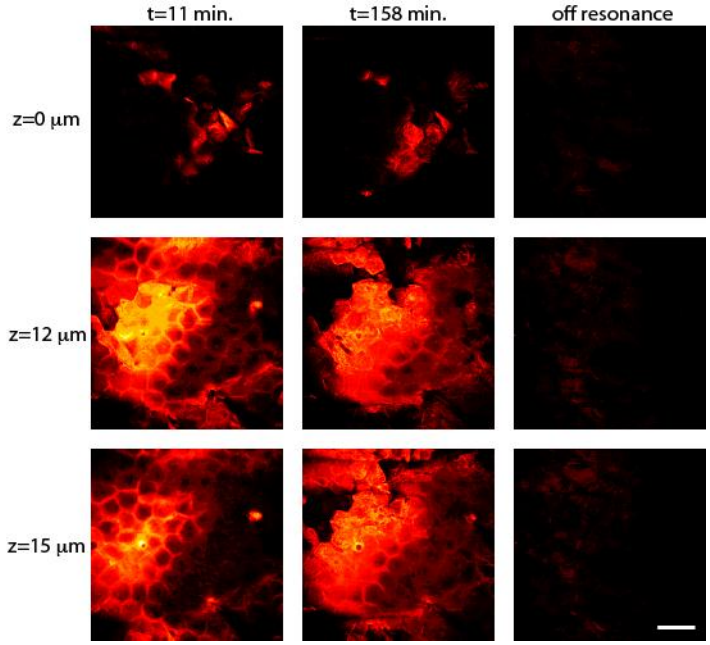

Figure 2*: Architecture of mouse skin based on SRS imaging. Images at t = 11 and 158 minutes are acquired with CH_2-stretching contrast and show the lipid architecture of the skin at various depths. The off resonance images demonstrate the chemical contrast of SRS. Scale bar = 50 μm.*

Then, on the same tissue sample, the laser was tuned either to the aromatic CH stretching absorbance frequency, or to the CD_2 (carbon-deuterium) stretching band to visualize ketoprofen and PG, respectively. Because it was possible to recognize individual cells in the skin, the 3-dimensional stacks could be registered to minimize the impact of drift and swelling of the tissue. This meant that changes in signal from the topically applied chemicals, as a function of depth within the SC, could be visualized throughout the experiment. Such time lapse images for deuterated PG and ketoprofen are in **Figure 3**. The image series at the skin surface (Z = 0 μm) shows minimal changes in intensity because the chemical concentrations above the tissue do not change significantly during the experiment. In contrast, images in the stratum corneum (Z = 12 and 15 μm) show increasing signal over time. The data acquisition time in these experiments was about 20 seconds per frame (256 x 256 pixels). Each stack of images from the skin surface to the deeper layers of the tissue therefore required about 10 minutes to acquire. Alternating stacks of images from the drug and from the cosolvent were obtained by re-tuning the laser between

each stack. It is apparent that both compounds penetrate via the intercellular lipids of the stratum corneum and, as well, through the hair shafts. Only by 3-dimensional resolution of the penetration maps is this type of direct mechanistic insight achievable, and other analytical techniques, including those based on spontaneous Raman scattering, lack sufficient spatiotemporal resolution for these measurements.

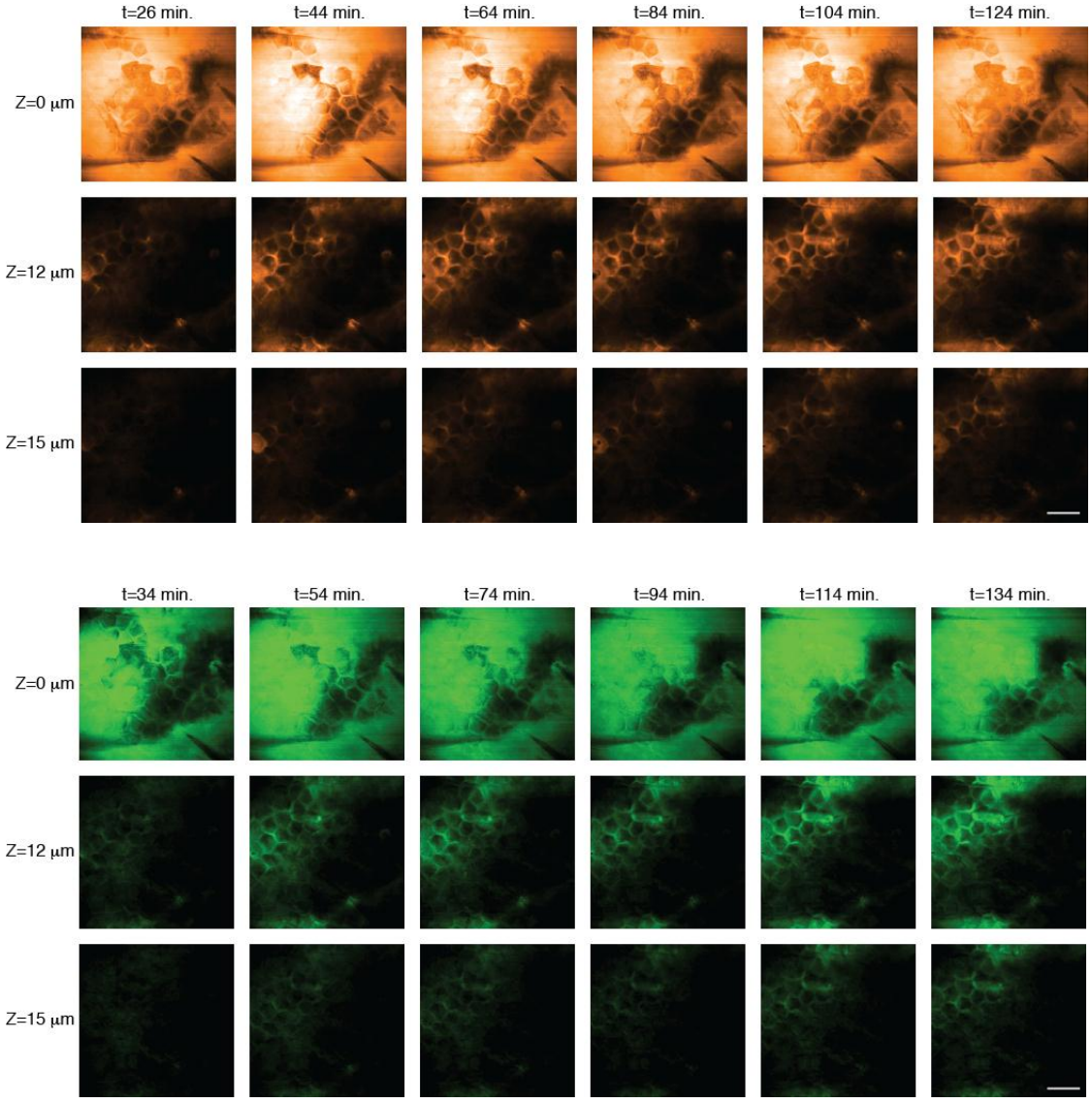

***Figure 3**: Imaging the penetration of deuterated PG (upper panel) and ketoprofen (lower panel) across the stratum corneum. Images acquired at the depths indicated down the left-hand side of the figure and times indicated along the top show the penetration of cosolvent and drug into the tissue using SRS contrast at 2120 cm^{-1} and 1599 cm^{-1}, respectively. Scale bar = 50 μm.*

Next, integration of the total signal as a function of depth from the registered 3-dimensional maps provided an effective concentration profile of the penetrating species. A representative result for deuterated PG as a function of time post-application of the formulation is in **Figure 4A**. Experimental data points were obtained by integrating comparable regions of interest in **Figure 3**. The relative amount of PG, as a function of position within the skin, at each time, is determined by the ratio of the integrated total signal at each depth to that at the surface (located at approximately Z = 0 µm). Thus, each normalized profile decreases from a value of 1 at the surface with increasing distance of penetration into the skin. Normalization of the profiles to 1 at the top layer assumes that the chemical's concentration above the sample does not change significantly during the experiment (a reasonable approximation given the effectively infinite 'dose' of solution applied at t = 0). Monotonically-increasing penetration profiles over time are observed; that is, the area under the normalized signal versus distance profiles increases as more of the cosolvent is absorbed into the SC.

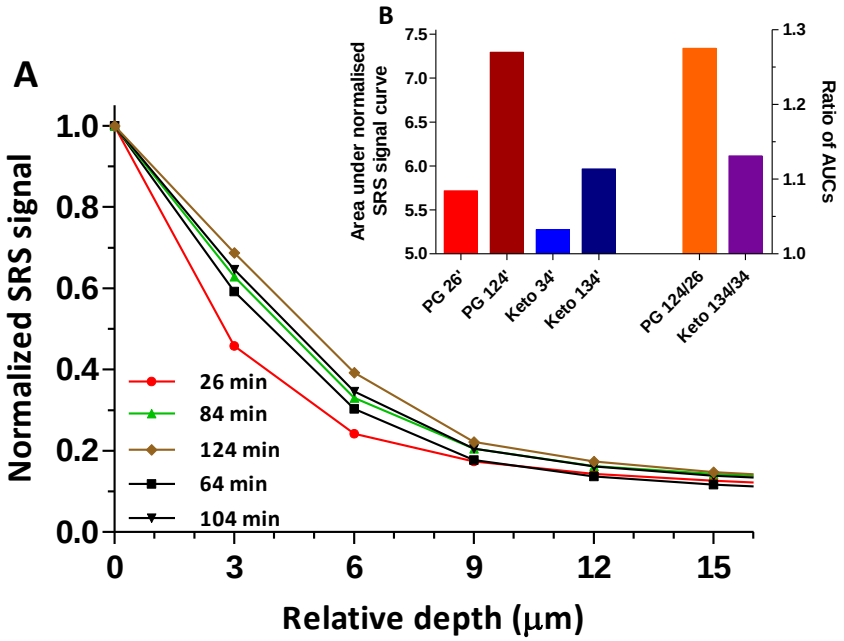

***Figure 4**: Integrated depth-profiling analysis of percutaneous penetration. **(A)** Depth profiles of deuterated PG as a function of time. **(B)** Comparison of the areas under the normalised SRS signal versus skin depth profiles (AUCs) of PG and ketoprofen at different times (26 and 104 minutes, and 34 and 134 minutes, respectively) post-application of the formulation (left-hand y-axis). The ratios of the AUCS (right-hand y-axis) determined after the first and last measurements (at approximately 0.5 and 2 hours) demonstrate the slower penetration rate of the drug compared to that of the cosolvent.*

Data obtained nearly simultaneously from ketoprofen showed similar behavior, although the slower rate of change of the normalized signal versus distance profile with increasing time demonstrated that PG penetrates the stratum corneum more efficiently than the drug (**Figure 4B**). This finding is consistent with tape-stripping and attenuated total reflectance infrared spectroscopy experiments that tracked the uptake of ibuprofen and PG into human SC[9-12], and emphasises the importance of tracking not only the drug when attempting to understand the performance of a topical formulation.[13] The temporal evolution of the effective concentration profiles in **Fig. 2A** and their monotonic decrease from the skin surface into the barrier are both qualitatively and quantitatively comparable with data from the far more invasive and labor-intensive tape-stripping results observed previously[9,11,12], and suggest a diffusion lag-time on the order of 2 hours. More refined interpretation of these results will be possible with the acquisition of SRS images in finer steps (e.g., 1 μm, rather than every 3 μm), and an improved use of the CH_2 signal to define SC thickness.

A major challenge in analyzing the 3-dimensional datasets presented here is to extract truly quantitative information from the images. Spatial drift and swelling of tissue over the time course of the experiment mean that the three-dimensional datasets must be registered with care in order to separate tissue movement from diffusion of the compounds of interest within the skin. In this work, this is achieved by visual inspection which permits linear 3-dimensional movements to be taken into account but cannot remove distortions or swelling of the tissue. In addition, the penetration of compounds, such as PG, can affect the linear optical properties of the tissue, affecting the depth profiles by changing signal levels because of alterations in laser power at the focus rather than changes in chemical concentration[14]. Recent reports of optical clearing measurements in microscopy suggest that these linear optical property changes are relatively rapid (they occur in ~30 minutes),[15] so that the measurements reported here, which began at 26 minutes post-initiation of the experiment, should not be significantly affected. Nevertheless, developing methods to compensate for the changing linear optical properties of tissue will improve quantitative analysis. Additionally, improving the imaging speed[7] will ultimately allow experiments to be conducted *in vivo*, where high speed imaging is a requirement because living samples inevitably move on the microscopic length scale, and result in blurred images if the acquisition speed is too low.

A further illustration of the ability of SRS microscopy to track chemical uptake and transport kinetics across the SC is illustrated in **Figure 5A**, which plots the normalized, integrated signal from PG at 12 and 15 μm from the skin surface (note that, in this case, the data have been normalized such that the

final value is equal to 1 so as to better visualize the overall trends with time). The significant increase in cosolvent level in deeper tissue layers with increasing time is clearly shown; in contrast, the relative signal at the skin surface (Z = 0 µm) did not change, reflecting the essentially infinite dose of formulation applied.

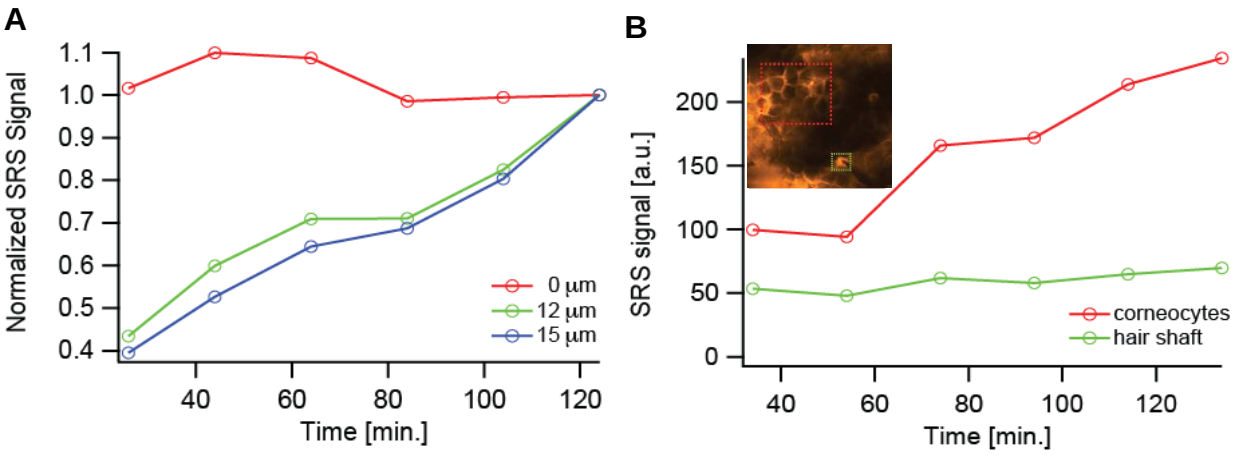

***Figure 5**: **(A)** Temporal profiles of the signal intensity from PG at the skin surface (Z = 0 µm) and at two representative depths (12 and 15 µm) into the skin. **(B)** Temporal profiles of PG at a depth of Z = 6 µm at two specific sub-regions of the images. The green trace corresponds to the area shown in the inset image enclosed by the green box that surrounds a hair shaft. The red trace corresponds to the area in the inset image enclosed by the red box that surrounds several corneocytes.*

In addition, the three-dimensional imaging capability provided novel mechanistic insight into the topical drug delivery process (an achievement impossible with Raman depth profiling[16,17] or tape stripping[2,9,11,12] which are essentially one-dimensional techniques). Specifically, **Figure 5B** compares the penetration profile of deuterated PG via a hair shaft to that via the SC intercellular lipids (outlined respectively in the inset of **Figure 5B** by the green and red boxes). These results were generated by integrating the signal from two regions of interest, one a clearly visible follicle, the other an area encompassing the basket-weave structure typical of SC, at the same depth, as a function of time. While the signal from SC steadily increased with time, that from the hair shaft remained essentially unchanged and, importantly, significantly above background. Thus, PG penetration via the hair shaft was rapid and attained steady-state before the first measurement was recorded at 26 minutes post-application of the formulation. On the other hand, transport through the SC intercellular lipids was slower and the increasing signal over time during the ~2-hour experiment represented the non-steady state approach to a constant flux. These data provide direct experimental proof of behavior deduced over 40 years ago by

Scheuplein[18,19] who inferred that the initial drug molecules crossing the skin post-treatment came through low-resistance, "shunt" pathways (such as hair shafts) of limited capacity; the parallel, but slower, transport across the bulk of the SC eventually overwhelms the transient pathways, however, and completely dominates at steady-state. Despite additional, indirect support for the importance of the follicular pathway,[20,21] the SRS microscopy data in **Figure 5B** are unique in their separation and real-time observation of molecular transport at two distinct rates occurring through two discrete and identifiable pathways across the skin.

In a final series of measurements, the apparently rapid penetration of the cosolvent, relative to that of drug (**Figure 4B**), was probed following topical application of deuterated ibuprofen in 'normal' (i.e., undeuterated) PG. The drug concentration in the cosolvent represented about 90% of its saturation solubility[9]. Less than 30 minutes post-application, the formation of solid ibuprofen crystals (with characteristic sizes of tens of microns - see **Figure 6A**), which produced a strong Raman signal at the CD stretching frequency, was observed at the skin surface (**Figure 6B**) on the SC (**Figure 6C**). Some drug penetration via the follicular "shunt" route was again seen (inset in **Figure 6B**). The logical explanation for the precipitation of ibuprofen observed is that the faster penetration of PG into the skin (coupled, perhaps, with some evaporation from the surface) caused the drug concentration to increase above its saturation solubility. Again, while this phenomenon has been anticipated, and for which indirect evidence has been obtained,[10] the 3-dimensional SRS imaging illustrated in **Figure 6** represents new and direct proof of the so-called "metamorphosis"[22-24] of a topical drug formulation post-application to the skin.

In summary, this SRS microscopy study of dermato-pharamacokinetics has revealed previously invisible features of the percutaneous penetration of skin-active compounds. As a label-free optical imaging technique, SRS permits non-destructive visualization of the drugs and excipients delivered from topically-applied formulations with high spatial and temporal resolution. The application of SRS to the delivery of ketoprofen and ibuprofen has unambiguously revealed distinct penetration pathways, across which the molecules transport at different rates, and has directly visualized the formation of drug crystals on the tissue surface *in situ* during the initial stages of the penetration process. Improved image acquisition speed, signal processing and analysis – especially in terms of defining more precisely the location of the skin surface - will allow further quantitative information to be extracted, and the technology may ultimately be applied *in vivo* (in models more relevant than the mouse skin used in this

work) to understand and optimize formulations and delivery vehicles for topical and transdermal drug delivery.

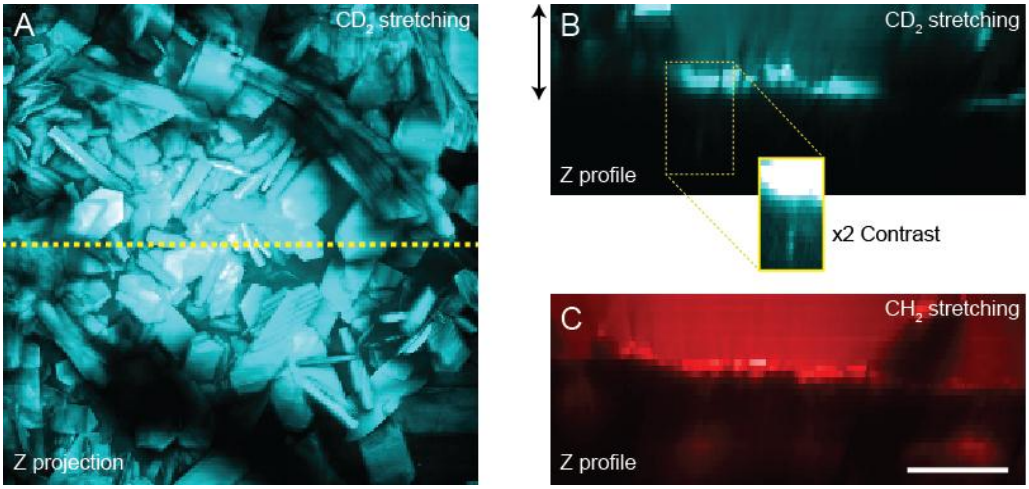

***Figure 6**: Crystal formation on the skin surface 25 minutes post-topical application of a solution of ibuprofen in PG. **(A)** Maximum intensity depth projection (of the upper ~30 µm) with SRS contrast at 2120 cm^{-1}. **(B)** Depth projection down the yellow dotted line in panel (A) again showing contrast for deuterated ibuprofen. Crystal formation on the tissue surface and some penetration down the hair shaft (inset) are seen. **(C)** CH_2-stretching image from the same region showed the bright SC and very clear contrast from the undeuterated PG above the SC. Scale bar = 50 µm.*

Acknowledgements

We thank C. Freudiger for helpful discussions. Funding for this work was provided by the Gates foundation and an NIH T-R01 grant (1R01EB010244-01) to X.S.X. L. R.C-R. is the recipient of a doctoral fellowship from CONACyT, Mexico. Patent applications based on SRS microscopy have been filed by Harvard University.

References

1. Williams, A.C. *Transdermal and Topical Drug Delivery from Theory to Clinical Practice*; Pharmaceutical Press: London, 2003.

2. Herkenne, C.; Alberti, I.; Naik, A.; Kalia, Y.N.; Mathy, F.X.; Préat, V.; Guy, R.H. *In vivo* methods for the assessment of topical drug bioavailability. Pharm. Res. **2008**, 25, 87-103.

3. Ploetz, E.; Laimgruber, S.; Berner, S.; Zinth, W.; Gilch, P. Femtosecond stimulated Raman microscopy. Appl. Phys. B: Las. Opt. 2007, 87, 389-393.

4. Freudiger, C.W.; Min, W.; Saar, B.G.; Lu, S.; Holtom, G.R.; He, C.; Tsai, J.C.; Kang, J.X.; Xie, X.S. Label-free biomedical imaging with high sensitivity by stimulated Raman scattering microscopy. Science **2008**, 322, 1857-1861.

5. Ozeki, Y.; Dake, F.; Kajiyama, S.; Fukui, K.; Itoh, K. Analysis and experimental assessment of the sensitivity of stimulated Raman scattering microscopy. Opt Express **2009**, 17, 3651-3658.

6. Nandakumar, P.; Kovalev, A.; Volkmer, A. Vibrational imaging based on stimulated Raman scattering microscopy. New J. Phys. **2009**, 11, 033026.

7. Saar, B.G.; Freudiger, C.W.; Reichman, J.; Stanley, C.M.; Holtom, G.R.; Xie, X.S. Video-rate molecular imaging in vivo with stimulated Raman scattering. Science **2010**, 330, 1368-1370.

8. Cho, Y.; Choi, H. Enhancement of percutaneous absorption of ketoprofen: effect of vehicles and adhesive matrix. Int. J. Pharm. **1998**, 169, 95-104.

9. Herkenne, C.; Naik, A.; Kalia, Y.N.; Hadgraft, J.; Guy, R.H. Effect of propylene glycol on ibuprofen absorption into human skin in vivo. J. Pharm. Sci. **2008**, 97, 185-197.

10. Nicoli, S.; Bunge, A.L.; Delgado-Charro, M.B.; Guy, R.H. Dermatopharmacokinetics: factors influencing drug clearance from the stratum corneum. Pharm. Res. **2009**, 26, 865-871.

11. Herkenne, C.; Naik, A.; Kalia, Y.N.; Hadgraft, J.; Guy, R.H. Ibuprofen transport into and through skin from topical formulations: *in vitro-in vivo* comparison. J. Invest. Dermatol. **2007**, 127, 135-142.

12. Herkenne, C.; Naik, A.; Kalia, Y.N.; Hadgraft, J.; Guy, R.H. Dermatopharmacokinetic prediction of topical drug bioavailability in vivo. J. Invest. Dermatol. **2007**, 127, 887-894.

13. Trottet, L.; Merly, C; Mirza, M; Hadgraft, J; Davis, A.F. Effect of finite doses of propylene glycol on enhancement of in vitro percutaneous permeation of loperamide hydrochloride. Int. J. Pharm. 2004, 274, 213-219.

14. Zimmerley, M.; McClure, R.A.; Choi, B.; Potma, E.O. Following dimethyl sulfoxide skin optical clearing dynamics with quantitative nonlinear multimodal microscopy. Appl. Opt. **2009**, 48, 79-87.

15. Genina, E.A.; Bashkatov, A.N.; Sinichkin, Y.P.; Tuchin, VV. Optical clearing of skin under action of glycerol: ex vivo and in vivo investigations. Opt. Spectrosc. **2010**, 109, 225-231.

16. Caspers, P.J.; Lucassen, G.W.; Carter, E.A.; Bruining, H.A.; Puppels, G.J. In vivo confocal Raman microspectroscopy of the skin: noninvasive determination of molecular concentration profiles. J. Invest. Dermatol. **2001**, 116, 434-442.

17. Pudney, P.; Mélot, M.; Caspers, P.; Van Der Pol, A.; Puppels, G. An in vivo confocal Raman study of the delivery of trans-retinol to the skin. Applied Spectroscopy **2007**, 61, 804-811.

18. Scheuplein, R.J. Mechanism of percutaneous adsorption. I. Routes of penetration and the influence of solubility. J. Invest. Dermatol. **1965**, 45, 334-346.

19. Scheuplein, R.J. Permeability of the skin: a review of major concepts and some new developments. J. Invest. Dermatol. **1976**, 67, 672-676.

20. Knorr, F.; Lademann, J.; Patzelt, A.; Sterry, W.; Blume-Peytavi, U.; Vogt, A. Follicular transport route: research progress and future perspectives. Eur. J. Pharm. Sci. **2009**, 71, 173-180.

21. Meidan, V.M. Methods for quantifying intrafollicular drug delivery: a critical appraisal. Expert Opin. Drug Deliv. **2010**, 7, 1095-1108.

22. Surber, C.; Davis, A.F. Bioavailability and bioequivalence of dermatological formulations. In *Dermatological and Transdermal Formulations*; Walters, K.A., Ed.; Informa Healthcare: New York, 2002; pp 401-498.

23. Santos, P.; Watkinson, A.C.; Hadgraft, J.; Lane, M.E. Enhanced permeation of fentanyl from supersaturated solutions in a model membrane. Int. J. Pharm. 2011, 407, 72-77.

24. Santos, P.; Watkinson, A.C.; Hadgraft, J.; Lane, M.E. Oxybutynin permeation in skin: The influence of drug and solvent activity. Int. J. Pharm. 2010, 384, 2010, 67-72.